Efficient Qubit Measurement with a Nonreciprocal Microwave Amplifier

F. Lecocq,[1,2,*] L. Ranzani,[3] G. A. Peterson,[1,2] K. Cicak,[1] X. Y. Jin,[1,2]
R. W. Simmonds,[1] J. D. Teufel,[1] and J. Aumentado[1,†]
[1]*National Institute of Standards and Technology, 325 Broadway, Boulder, Colorado 80305, USA*
[2]*Department of Physics, University of Colorado, 2000 Colorado Avenue, Boulder, Colorado 80309, USA*
[3]*Raytheon BBN Technologies, Cambridge, Massachusetts 02138, USA*

(Received 1 September 2020; accepted 7 December 2020; published 13 January 2021)

The act of observing a quantum object fundamentally perturbs its state, resulting in a random walk toward an eigenstate of the measurement operator. Ideally, the measurement is responsible for all dephasing of the quantum state. In practice, imperfections in the measurement apparatus limit or corrupt the flow of information required for quantum feedback protocols, an effect quantified by the measurement efficiency. Here, we demonstrate the efficient measurement of a superconducting qubit using a nonreciprocal parametric amplifier to directly monitor the microwave field of a readout cavity. By mitigating the losses between the cavity and the amplifier, we achieve a measurement efficiency of $(72 \pm 4)\%$. The directionality of the amplifier protects the readout cavity and qubit from excess backaction caused by amplified vacuum fluctuations. In addition to providing tools for further improving the fidelity of strong projective measurement, this work creates a test bed for the experimental study of ideal weak measurements, and it opens the way toward quantum feedback protocols based on weak measurement such as state stabilization or error correction.

DOI: 10.1103/PhysRevLett.126.020502

Quantum measurements often involve entangling the system of interest with light [1]. As a consequence, the subsequent measurement of the light, performed by an observer or by the unmonitored environment, affects the quantum state of the system [2]. The measurement efficiency $0 \leq \eta \leq 1$ characterizes the fraction of the total available quantum state information that is acquired by the observer. Using a quantum nondemolition measurement scheme, highly accurate state estimation can be performed by repeating many inefficient measurements [3–5]. A higher efficiency results in measurement speed up and, therefore, contributes to the fidelity of the state estimation, a crucial metric for quantum computation [6,7]. Meanwhile, an efficient measurement is critical for measurement-based quantum control [8], in which the measurement outcome is used to feed back on the quantum system, enabling, for example, quantum state stabilization [9–12] or measurement-based entanglement [13].

A perfectly efficient measurement requires both ideal collection of the light and a faithful, noiseless detector. For superconducting qubits, the use of a microwave readout resonator with a one-dimensional radiation pattern enables the collection of every photon [14]. A noiseless detector must measure only the information-carrying quadrature of the microwave field, and, in principle, this can be implemented with a phase-sensitive parametric amplifier [15]. In reality, this approach requires additional hardware to operate which introduces unavoidable losses in the signal path, reducing the overall efficiency. In particular, these amplifiers are reciprocal and, therefore, rely on magnetic microwave circulators to control the signal flow, leading to significant component and wiring losses [16,17]. In recent years, various nonreciprocal alternatives to conventional parametric amplifiers have been developed, breaking reciprocity via parametric interactions [18–23], time-domain operations [24], or traveling wave amplification [25]. However, the application of these nonreciprocal amplifiers to efficient superconducting qubit measurement is still a nascent field [24,26–29] with many outstanding experimental and theoretical challenges. Indeed, in the absence of an intermediate circulator, the amplifier and the device under test can no longer be treated as independent modular elements, in stark contrast with conventional parametric amplification chains. In fact, the devices merge into a new and unique quantum system, which introduces the difficulty of combining large amplified signals with fragile quantum states. In this work, we solve this delicate balance by using coupled mode theory to finely tune *in situ* parametric interference within this larger quantum system.

Here, we couple the readout cavity of a transmon qubit to a field programmable Josephson amplifier (FPJA) [22]; see Fig. 1. We operate the FPJA as a directional phase-sensitive parametric amplifier [23] to monitor only the quadrature of the microwave field in which the qubit state is encoded. The directionality of the amplifier protects the cavity from amplified vacuum fluctuations, circumventing the need for conventional microwave circulators between the cavity and the amplifier. As a consequence of the low loss and low added

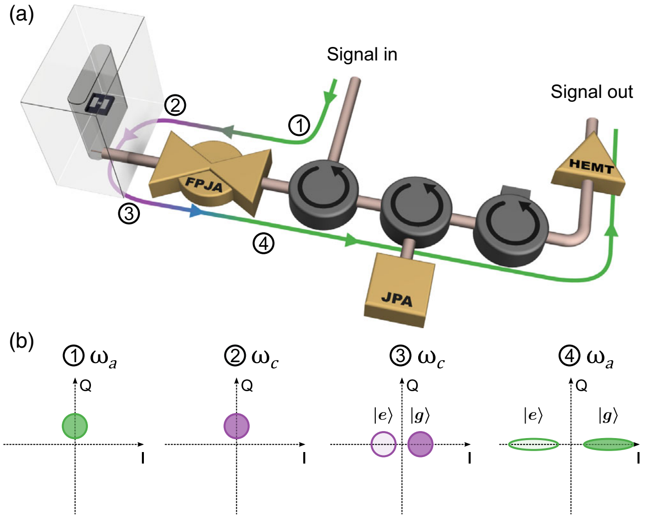

FIG. 1. (a) Diagram of the high-efficiency qubit measurement chain. A transmon qubit is dispersively coupled to a 3D aluminum readout cavity. The readout cavity is directly connected to a nonreciprocal phase-sensitive amplifier based on an FPJA. (b) Phase-space representation of the microwave field at different parts of the circuit. An input measurement drive is up-converted to the cavity frequency and then reflected with a qubit state-dependent phase shift. The quadrature containing the qubit state information is amplified, and the signal is down-converted and routed out for further amplification. Both the FPJA and the JPA have an on-chip dc and ac flux bias (not shown). The qubit is driven via a weakly coupled cavity port (not shown).

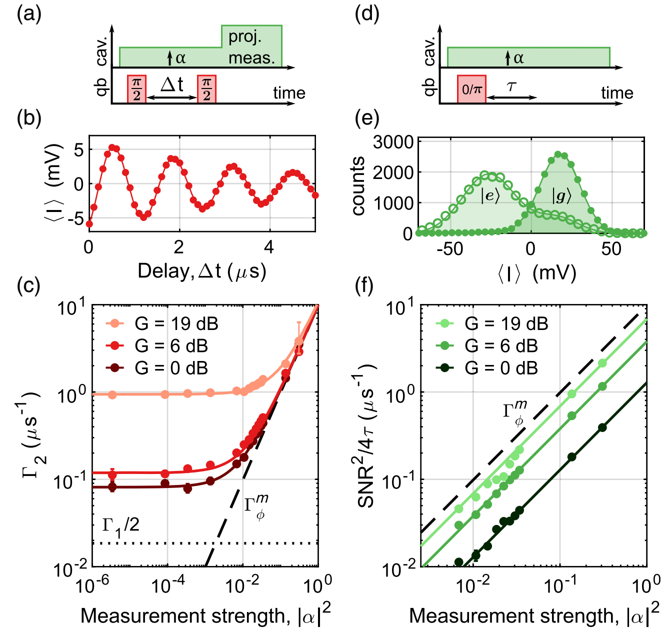

FIG. 2. Measurement-induced dephasing and measurement rate. (a) Pulse sequence to measure Ramsey oscillations in the presence of a measurement of variable strength $|\alpha|^2$. (b) Example of a Ramsey oscillation with an exponential decay rate Γ_2, for $G \approx 6$ dB and $|\alpha|^2 \approx 0.01$. (c) Qubit decoherence rate Γ_2 as a function of measurement strength $|\alpha|^2$ and amplifier gain G. (d) Pulse sequence to measure the signal to noise ratio between the ground and excited qubit state as a function of the measurement strength $|\alpha|^2$. (e) Typical histogram of the measurement signal for the qubit prepared in the ground or excited state, for $G \approx 15$ dB and $|\alpha|^2 \approx 0.3$. (f) Measurement rate $\Gamma_m = \mathrm{SNR}^2/4\tau$ as a function of measurement strength $|\alpha|^2$ and amplifier gain G. In (b), (c), (e), and (f), the dots are data, and the solid lines are linear fits.

noise in this system, we achieve a measurement efficiency of $(72 \pm 4)\%$, among the best reported in the literature [6,24,28].

A transmon qubit, with a resonance frequency $\omega_q/2\pi \approx 6.297$ GHz and relaxation time $T_1 = 27\ \mu$s, is embedded inside a three-dimensional aluminum readout cavity [30] with a resonant frequency $\omega_r/2\pi \approx 10.929$ GHz. The capacitive coupling between the qubit and the cavity results in a qubit state-dependent cavity resonance frequency: $\omega_r + \chi$ or $\omega_r - \chi$ for the qubit, respectively, in the ground state $|g\rangle$ or excited state $|e\rangle$, where $2\chi/2\pi \approx 1.7$ MHz. The FPJA is part of a class of multimode amplifiers whose behavior can be programmed *in situ* by a set of parametric drives [18–20,22]. In the following, we use four parametric drives to program the FPJA as a directional phase-sensitive amplifier [23]. The FPJA has three flux-tunable resonances: The input resonator is tuned into resonance with the readout cavity, $\omega_c = \omega_r$, resulting in an output resonator frequency $\omega_a/2\pi \approx 6.912$ GHz and an internal amplification resonator frequency $\omega_b/2\pi \approx 8.013$ GHz (see Supplemental Material [31]). The strength and phase of each pump are set to create the following nonreciprocal signal flow: (i) A signal enters the FPJA output port, at a frequency ω_a; (ii) the signal is up-converted to the input port of the FPJA, at a frequency ω_c; (iii) the signal reflects off the readout cavity with a qubit state-dependent phase shift and reenters the FPJA input port; (iv) the signal is down-converted to the amplification resonator, at a frequency ω_b, and the quadrature containing the qubit state information is amplified with a gain G tunable *in situ* before further down-conversion back to the output port, at a frequency ω_a. Finally, the signal is routed to a conventional homodyne measurement setup. To characterize this system's measurement efficiency, we use a robust method that relies on the comparison of the qubit dephasing rate to the measurement rate [24,28,32,33].

We first calibrate the qubit measurement strength by observing the associated measurement-induced dephasing; see Figs. 2(a)–2(c). The total qubit decoherence rate is $\Gamma_2 = \Gamma_1/2 + \Gamma_\phi^{\mathrm{env}} + \Gamma_\phi^m$, where Γ_1 is the relaxation rate, Γ_ϕ^m is the measurement-induced dephasing rate, and $\Gamma_\phi^{\mathrm{env}}$ is the excess dephasing rate that is not due to the measurement. Both dephasing rates can be expressed as a function of the number of photons in the cavity [34,35]:

$$\Gamma_\phi^{\mathrm{env}} = \frac{4\chi^2\kappa}{4\chi^2 + \kappa^2} n_{\mathrm{env}},$$

$$\Gamma_\phi^m = \frac{8\chi^2\kappa}{4\chi^2 + \kappa^2} |\alpha|^2, \tag{1}$$

where $\kappa/2\pi \approx 2.58$ MHz is the effective cavity linewidth, n_{env} is the effective thermal occupancy of the cavity, and $|\alpha|^2$ is the mean number of coherent photons that parameterizes the measurement strength. Using the Ramsey sequence shown in Fig. 2(a), we measure the qubit decoherence rate Γ_2 as a function of the measurement strength $|\alpha|^2$ and of the FPJA gain G, shown in Fig. 2(c). The measurement strength $|\alpha|^2$ is calibrated using Eq. (1) and separate measurements of κ and χ. At low measurement strength, the qubit decoherence rate is mostly dominated by excess dephasing $\Gamma_\phi^{\mathrm{env}}$. At zero gain, $\Gamma_\phi^{\mathrm{env}}$ originates from residual thermal photons in the cavity [35]. At higher gain, due to the finite directionality of the FPJA, residual amplified vacuum fluctuations drive the readout cavity and slightly increase the excess dephasing. The decoherence rate then increases with measurement strength, and even at the highest gain we maintain a measurement-induced dephasing rate that dominates the decoherence rate, $\Gamma_\phi^m \gg (\Gamma_1/2 + \Gamma_\phi^{\mathrm{env}})$.

We now extract the signal to noise ratio (SNR) of the measurement chain; see Figs. 2(d)–2(f). The measurement signal after an integration time τ consists of two Gaussian distributions corresponding to the ground and excited qubit states, with mean values $\langle I_{g,e}\rangle$, standard deviations $\sigma_{g,e}$, and $\mathrm{SNR}^2 = (\langle I_g\rangle - \langle I_e\rangle)^2/(\sigma_g^2 + \sigma_e^2)$; see Fig. 2(d). Experimentally, we prepare the qubit in either its ground or excited state and measure the rate at which the SNR grows as a function of the integration time ($\tau \gg 1/\kappa$), yielding the measurement rate $\Gamma_m = \mathrm{SNR}^2/4\tau$ [36]. In Fig. 2(f), we show the measurement rate as a function of the measurement strength and FPJA gain. As expected, the SNR increases linearly with the measurement amplitude, $|\alpha|$. As the FPJA gain increases, the measurement rate approaches the measurement-induced dephasing rate (dashed line), a hallmark of a highly efficient measurement.

The ratio of the measurement rate to the measurement-induced dephasing rate yields the measurement efficiency $\eta_m = \Gamma_m/\Gamma_\phi^m$ [36], shown in Fig. 3 as a function of the FPJA gain. At low FPJA gain, the measurement efficiency is limited by the system noise temperature of the homodyne measurement setup (Supplemental Material [31]). As the FPJA gain increases, it overwhelms the noise of the homodyne setup, and the efficiency increases. Concurrently, the thermal occupancy of the cavity, n_{env}, increases slightly, as discussed previously in Fig. 2. This results in an increase of the photon shot noise in the cavity and, therefore, of the qubit dephasing, which can be cast as an environmental efficiency [10] $\eta_{\mathrm{env}} = 1/(1 + 2n_{\mathrm{env}})$, shown in Fig. 3. At an optimal gain of approximately 15 dB, we reach an efficiency of $\eta_m = (72 \pm 4)\%$ and an environmental efficiency $\eta_{\mathrm{env}} = (88 \pm 2)\%$. An empirical noise model suggests that η_m is primarily limited by residual coupling of the amplifier resonance to the output port [23]. Both the measurement inefficiency $1 - \eta_m$ and thermal occupancy of the cavity n_{env} can be reduced by at least an order of magnitude with a straightforward redesign of the external coupling to each resonator of the FPJA [23]. We note that the small discrepancy between the measured backaction and theoretical predictions is potentially due to a weak measurement performed by the amplifier even in the absence of cavity displacement. Indeed, the state-dependent frequency shift of the readout cavity results in a state-dependent gain profile of the amplifier. As a consequence, the qubit state is encoded in the output noise spectrum which, if unmonitored, results in spurious dephasing. This form of backaction has been observed in other experiments and is an active area of research [28,37].

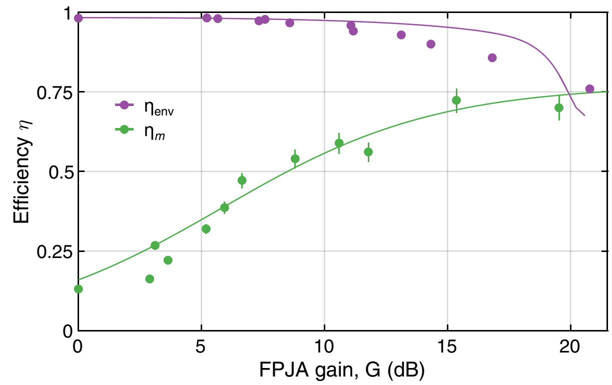

FIG. 3. Measurement efficiency η_m, in green, and environmental efficiency η_{env}, in purple, as a function of the amplifier gain. The solid green line is the prediction of an empirical noise model for the measurement efficiency, and the solid purple line is the theoretical prediction for the environmental efficiency (see Supplemental Material [31]). At high FPJA gain, the measurement efficiency clearly exceeds the 50% theoretical limit for a phase-insensitive amplifier.

At the optimal FPJA gain, we demonstrate the ability to perform strong projective qubit measurements. We extract a state-estimation fidelity of 97% in 350 ns for $|\alpha|^2 \approx 2.5$, mostly dominated by the ratio of the qubit relaxation rate and the cavity linewidth (Supplemental Material [31]). The dynamic range of the amplifier is large enough for a measurement strength $|\alpha|^2 > 5$, approaching the limits of the dispersive approximation [38], inducing spurious qubit transitions.

In conclusion, we have demonstrated a highly efficient measurement of a transmon qubit using a parametrically driven, directional, phase-sensitive amplifier connected to the readout cavity without an intermediate circulator. As in other work [24,27–29], our approach strives to achieve a high level of integration with superconducting quantum devices. While direct on-chip integration could be feasible, a flip-chip [39] or wireless coupling [40] approach would enable separate optimization of the amplifier and qubit chips. Straightforward adjustments of device parameters will enable measurement efficiencies approaching 100%, creating a test bed for exploring quantum control protocols based on weak continuous measurement. In addition, we emphasize that the FPJA can be dynamically reconfigured, enabling complex time-domain protocols with tunable control, coupling, and measurement of multiple quantum systems.

We thank E. Rosenthal and B. Hauer for helpful discussions and comments on the manuscript.

[*]florent.lecocq@nist.gov
[†]jose.aumentado@nist.gov

[1] V. B. Braginsky, F. Y. Khalili, and K. S. Thorne, *Quantum Measurement* (Cambridge University Press, Cambridge, England, 1992).

[2] S. Haroche and J. M. Raimond, *Exploring the Quantum: Atoms, Cavities, and Photons* (Oxford University Press, Oxford, 2006).

[3] T. P. Harty, D. T. C. Allcock, C. J. Ballance, L. Guidoni, H. A. Janacek, N. M. Linke, D. N. Stacey, and D. M. Lucas, High-Fidelity Preparation, Gates, Memory, and Readout of a Trapped-Ion Quantum Bit, Phys. Rev. Lett. **113**, 220501 (2014).

[4] S. S. Elder, C. S. Wang, P. Reinhold, C. T. Hann, K. S. Chou, B. J. Lester, S. Rosenblum, L. Frunzio, L. Jiang, and R. J. Schoelkopf, High-Fidelity Measurement of Qubits Encoded in Multilevel Superconducting Circuits, Phys. Rev. X **10**, 011001 (2020).

[5] S. L. Todaro, V. B. Verma, K. C. McCormick, D. T. C. Allcock, R. P. Mirin, D. J. Wineland, S. W. Nam, A. C. Wilson, D. Leibfried, and D. H. Slichter, State readout of a trapped ion qubit using a trap-integrated superconducting photon detector, arXiv:2008.00065 [Phys. Rev. Lett. (to be published)].

[6] T. Walter, P. Kurpiers, S. Gasparinetti, P. Magnard, A. Potočnik, Y. Salathé, M. Pechal, M. Mondal, M. Oppliger, C. Eichler, and A. Wallraff, Rapid high-fidelity single-shot dispersive readout of superconducting qubits, Phys. Rev. Applied **7**, 054020 (2017).

[7] F. Arute *et al.*, Quantum supremacy using a programmable superconducting processor, Nature (London) **574**, 505 (2019).

[8] H. M. Wiseman and G. J. Milburn, *Quantum Measurement and Control* (Cambridge University Press, Cambridge, England, 2009).

[9] C. Sayrin, I. Dotsenko, X. Zhou, B. Peaudecerf, T. Rybarczyk, S. Gleyzes, P. Rouchon, M. Mirrahimi, H. Amini, M. Brune, J.-M. Raimond, and S. Haroche, Real-time quantum feedback prepares and stabilizes photon number states, Nature (London) **477**, 73 (2011).

[10] R. Vijay, C. Macklin, D. H. Slichter, S. J. Weber, K. W. Murch, R. Naik, A. N. Korotkov, and I. Siddiqi, Stabilizing Rabi oscillations in a superconducting qubit using quantum feedback, Nature (London) **490**, 77 (2012).

[11] G. de Lange, D. Ristè, M. J. Tiggelman, C. Eichler, L. Tornberg, G. Johansson, A. Wallraff, R. N. Schouten, and L. DiCarlo, Reversing Quantum Trajectories with Analog Feedback, Phys. Rev. Lett. **112**, 080501 (2014).

[12] M. Rossi, D. Mason, J. Chen, Y. Tsaturyan, and A. Schliesser, Measurement-based quantum control of mechanical motion, Nature (London) **563**, 53 (2018).

[13] N. Roch, M. E. Schwartz, F. Motzoi, C. Macklin, R. Vijay, A. W. Eddins, A. N. Korotkov, K. B. Whaley, M. Sarovar, and I. Siddiqi, Observation of Measurement-Induced Entanglement and Quantum Trajectories of Remote Superconducting Qubits, Phys. Rev. Lett. **112**, 170501 (2014).

[14] A. A. Houck, D. I. Schuster, J. M. Gambetta, J. A. Schreier, B. R. Johnson, J. M. Chow, L. Frunzio, J. Majer, M. H. Devoret, S. M. Girvin, and R. J. Schoelkopf, Generating single microwave photons in a circuit, Nature (London) **449**, 328 (2007).

[15] C. M. Caves, Quantum limits on noise in linear amplifiers, Phys. Rev. D **26**, 1817 (1982).

[16] L. Ranzani, L. Spietz, Z. Popovic, and J. Aumentado, Two-port microwave calibration at millikelvin temperatures, Rev. Sci. Instrum. **84**, 034704 (2013).

[17] J. Aumentado, Superconducting parametric amplifiers: The state of the art in Josephson parametric amplifiers, IEEE Microw. Mag. **21**, 45 (2020).

[18] L. Ranzani and J. Aumentado, Graph-based analysis of nonreciprocity in coupled-mode systems, New J. Phys. **17**, 023024 (2015).

[19] A. Metelmann and A. A. Clerk, Nonreciprocal Photon Transmission and Amplification via Reservoir Engineering, Phys. Rev. X **5**, 021025 (2015).

[20] K. M. Sliwa, M. Hatridge, A. Narla, S. Shankar, L. Frunzio, R. J. Schoelkopf, and M. H. Devoret, Reconfigurable Josephson Circulator/Directional Amplifier, Phys. Rev. X **5**, 041020 (2015).

[21] B. J. Chapman, E. I. Rosenthal, J. Kerckhoff, B. A. Moores, L. R. Vale, J. A. B. Mates, G. C. Hilton, K. Lalumière, A. Blais, and K. W. Lehnert, Widely Tunable On-Chip Microwave Circulator for Superconducting Quantum Circuits, Phys. Rev. X **7**, 041043 (2017).

[22] F. Lecocq, L. Ranzani, G. A. Peterson, K. Cicak, R. W. Simmonds, J. D. Teufel, and J. Aumentado, Nonreciprocal microwave signal processing with a field-programmable Josephson amplifier, Phys. Rev. Applied **7**, 024028 (2017).

[23] F. Lecocq, L. Ranzani, G. A. Peterson, K. Cicak, A. Metelmann, S. Kotler, R. W. Simmonds, J. D. Teufel, and J. Aumentado, Microwave measurement beyond the quantum limit with a nonreciprocal amplifier, Phys. Rev. Applied **13**, 044005 (2020).

[24] E. I. Rosenthal, C. M. F. Schneider, M. Malnou, Z. Zhao, F. Leditzky, B. J. Chapman, W. Wustmann, X. Ma, D. A. Palken, M. F. Zanner, L. R. Vale, G. C. Hilton, J. Gao, G. Smith, G. Kirchmair, and K. W. Lehnert, Efficient and low-backaction quantum measurement using a chip-scale detector, arXiv:2008.03805.

[25] C. Macklin, K. O'Brien, D. Hover, M. E. Schwartz, V. Bolkhovsky, X. Zhang, W. D. Oliver, and I. Siddiqi, A near quantum-limited Josephson traveling-wave parametric amplifier, Science **350**, 307 (2015).

[26] B. Abdo, K. Sliwa, S. Shankar, M. Hatridge, L. Frunzio, R. Schoelkopf, and M. Devoret, Josephson Directional Amplifier for Quantum Measurement of Superconducting Circuits, Phys. Rev. Lett. **112**, 167701 (2014).

[27] T. Thorbeck, S. Zhu, E. Leonard, R. Barends, J. Kelly, J. M. Martinis, and R. McDermott, Reverse isolation and backaction of the SLUG microwave amplifier, Phys. Rev. Applied **8**, 054007 (2017).

[28] A. Eddins, J. M. Kreikebaum, D. M. Toyli, E. M. Levenson-Falk, A. Dove, W. P. Livingston, B. A. Levitan, L. C. G. Govia, A. A. Clerk, and I. Siddiqi, High-Efficiency Measurement of an Artificial Atom Embedded in a Parametric Amplifier, Phys. Rev. X **9**, 011004 (2019).
[29] B. Abdo, O. Jinka, N. T. Bronn, S. Olivadese, and M. Brink, On-chip single-pump interferometric Josephson isolator for quantum measurements, arXiv:2006.01918.
[30] H. Paik, D. I. Schuster, L. S. Bishop, G. Kirchmair, G. Catelani, A. P. Sears, B. R. Johnson, M. J. Reagor, L. Frunzio, L. I. Glazman, S. M. Girvin, M. H. Devoret, and R. J. Schoelkopf, Observation of High Coherence in Josephson Junction Qubits Measured in a Three-Dimensional Circuit QED Architecture, Phys. Rev. Lett. **107**, 240501 (2011).
[31] See Supplemental Material at http://link.aps.org/supplemental/10.1103/PhysRevLett.126.020502 for additional experimental details.
[32] C. C. Bultink, B. Tarasinski, N. Haandbæk, S. Poletto, N. Haider, D. J. Michalak, A. Bruno, and L. DiCarlo, General method for extracting the quantum efficiency of dispersive qubit readout in circuit QED, Appl. Phys. Lett. **112**, 092601 (2018).
[33] S. Touzard, A. Kou, N. E. Frattini, V. V. Sivak, S. Puri, A. Grimm, L. Frunzio, S. Shankar, and M. H. Devoret, Gated Conditional Displacement Readout of Superconducting Qubits, Phys. Rev. Lett. **122**, 080502 (2019).
[34] J. Gambetta, A. Blais, M. Boissonneault, A. A. Houck, D. I. Schuster, and S. M. Girvin, Quantum trajectory approach to circuit QED: Quantum jumps and the Zeno effect, Phys. Rev. A **77**, 012112 (2008).
[35] Z. Wang, S. Shankar, Z. K. Minev, P. Campagne-Ibarcq, A. Narla, and M. H. Devoret, Cavity attenuators for superconducting qubits, Phys. Rev. Applied **11**, 014031 (2019).
[36] N. Didier, J. Bourassa, and A. Blais, Fast Quantum Nondemolition Readout by Parametric Modulation of Longitudinal Qubit-Oscillator Interaction, Phys. Rev. Lett. **115**, 203601 (2015).
[37] G. Liu, X. Cao, T. C. Chien, C. Zhou, P. Lu, and M. Hatridge, Noise reduction in qubit readout with a two-mode squeezed interferometer, arXiv:2007.15460.
[38] A. Blais, R. S. Huang, A. Wallraff, S. M. Girvin, and R. J. Schoelkopf, Cavity quantum electrodynamics for superconducting electrical circuits: An architecture for quantum computation, Phys. Rev. A **69**, 062320 (2004).
[39] D. Rosenberg, D. Kim, R. Das, D. Yost, S. Gustavsson, D. Hover, P. Krantz, A. Melville, L. Racz, G. O. Samach, S. J. Weber, F. Yan, J. L. Yoder, A. J. Kerman, and W. D. Oliver, 3D integrated superconducting qubits, npj Quantum Inf. **3**, 42 (2017).
[40] Y. Y. Gao, B. J. Lester, K. S. Chou, L. Frunzio, M. H. Devoret, L. Jiang, S. M. Girvin, and r. J. Schoelkopf, Entanglement of bosonic modes through an engineered exchange interaction, Nature (London) **566**, 509 (2019).